

# GM-APD Imaging Arrays for Direct Imaging of Exoplanets

Kimberly Kolb  
Center for Detectors  
Rochester Institute of Technology  
Engineering Hall, Building 17, Room 3177  
74 Lomb Memorial Drive  
Rochester, NY 14623  
585-475-2338  
kem2691@rit.edu

Donald F. Figer  
Center for Detectors  
Rochester Institute of Technology  
Engineering Hall, Building 17, Room 3153  
74 Lomb Memorial Drive  
Rochester, NY 14623  
585-475-6005  
figer@cf.d.rit.edu

*Abstract*—Exoplanet detection and characterization is one of NASA's main science goals. Current missions, such as Kepler, are identifying exoplanet candidates for further study at an unprecedented pace. The upcoming Wide Field InfraRed Survey Telescope (WFIRST) mission is the top-ranked large space mission in the New World New Horizons decadal survey, and will "settle essential questions" in exoplanet research. This paper evaluates photon-counting Geiger-mode avalanche photodiode (GM-APD) imaging arrays for use in the WFIRST Astrophysics Focused Telescope Assets (AFTA) mission design, specifically in the area of direct imaging of exoplanets. A review of both current and state-of-the-art performance for GM-APD devices is presented, including the effects of radiation damage on device performance. Projected performance for next-generation devices is presented based on preliminary testing and state-of-the-art benchmarks for the technology. Simulated data for typical exoplanet signals is used to compare GM-APD performance with a state-of-the-art electron-multiplying charge coupled device (EMCCD), a current candidate for the WFIRST-AFTA mission.

characterization of the planet with exposures that are optimized for the exoplanet signal. The telescope observes the planet during its orbit, detecting the light reflected off of the planet from the star while not in transit. Coronagraphs have enabled high-quality direct imaging by blocking light from the star. The Hubble Space Telescope (HST) has used a coronagraph to image the nebulosity around bright stars since 1998 [2]. Other missions have also been proposed with a coronagraph as a key component, as on NASA's Terrestrial Planet Finder coronagraph [3]. The proposed WFIRST-AFTA mission currently includes a coronagraph instrument. The details of this proposed instrument provide a convenient way to compare the performance of two detector types for direct imaging applications.

## TABLE OF CONTENTS

1. INTRODUCTION .....	1
2. WFIRST-AFTA CORONAGRAPH .....	1
3. GM-APD DEVICE OVERVIEW .....	2
4. EXOPLANET DETECTION SIMULATIONS	4
5. CONCLUSIONS .....	6
REFERENCES.....	8
BIOGRAPHY .....	9

## 2. WFIRST-AFTA CORONAGRAPH

WFIRST-AFTA uses a coronagraph instrument to block light from the star and directly image the orbiting exoplanet. The mission will give the first reflected (visible) light images of the planetary systems of nearby stars [4].

### *Imaging Capabilities*

The 2.4 m aperture provides a total field of  $0.4^\circ$ . The coronagraph has an inner working angle of 100 mas, equivalent to 1 AU at 10 pc, and an outer working angle of 750 mas. The instrument is designed to image planets that have a planet:star contrast of  $5 \times 10^{-10}$  to  $5 \times 10^{-8}$ , focusing on bright stars. The wavelength range of the instrument is 400 nm - 1000 nm [4].

## 1. INTRODUCTION

Exoplanet detection and characterization is a burgeoning field in astronomy. With the Kepler mission identifying exoplanet candidates at an unprecedented pace, more advanced imaging and spectroscopic capabilities are required to confirm exoplanets and study them in detail. Direct imaging is not as constrained by orbital paths as transit photometry [1] and enables detailed spectroscopic

### *Candidate Imaging Detectors*

Direct imaging requires sensitive detectors with very low noise. The best detector candidates are detectors with zero read noise (photon-counting), high efficiency, and low dark current. GM-APD array-based imaging detectors are promising for future missions. The operational and performance details of such a detector are discussed in this paper.

One of the current detector candidates for the WFIRST-AFTA coronagraph instrument is an e2v CCD201-20, a photon-counting EMCCD with 1k x 1k pixels. The detector has a dark current of 0.0003 e-/pix/s and a clock-induced charge (CIC) of 0.001 e-/pix/frame, and the quantum efficiency (QE) in the V-band (550 nm) is 93%. The read noise when operated at modest frame rates is 8 e<sup>-</sup> rms, which is effectively 0.04 e<sup>-</sup> rms at a gain of 200 (suggested gain value). The gain is provided by 604 multiplication elements in the readout register [5].

To evaluate the performance of GM-APDs for a mission such as WFIRST-AFTA, the EMCCD described above will be used as a basis of comparison.

### 3. GM-APD DEVICE OVERVIEW

The array-based GM-APDs discussed here have been developed by the Massachusetts Institute of Technology Lincoln Laboratory and characterized by the Center for Detectors to determine their suitability for space-based imaging applications, specifically for exoplanet missions [6]. Figure 1 shows a cross-sectional view of a single pixel in a GM-APD device.

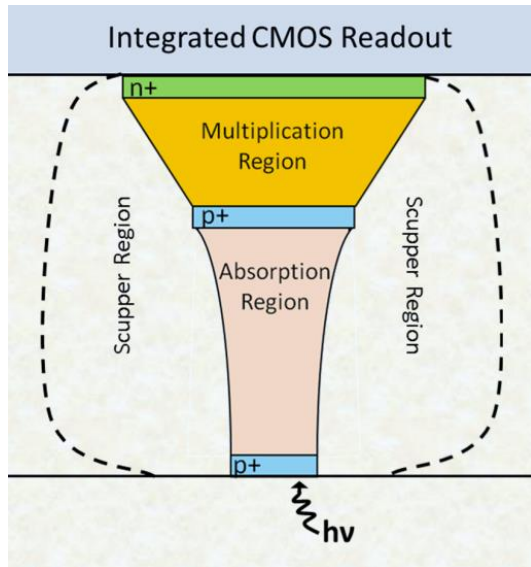


**Figure 1. This figure shows the GM-APD design for one pixel (not to scale).**

The bulk material is very lightly doped (nearly intrinsic) silicon, and the implants (noted “p+” and “n+” in the figure) have a high dopant concentration and are very narrow. Each pixel in the device is made up of three distinct regions, each with a specific function. The absorber region has a medium-strength electric field that moves carriers to the multiplier region, which has a strong electric field (above the

critical field required for avalanche breakdown) to facilitate avalanches. A weak electric field, called a “scupper,” surrounds the absorption and multiplication regions of each pixel to direct carriers generated outside of these regions to the cathode without initiating an avalanche. This reduces the dark count rate (the number of dark current carriers that initiate an avalanche per pixel per second) [7].

#### Device Operation

The GM-APD detector described here measures intensity by measuring the avalanche probability during a short exposure window (usually on the order of microseconds), similarly to EMCCDs in photon-counting mode.

The detection cycle of the devices is clocked externally and reset at regular intervals. Each exposure is comprised of five distinct stages, repeated many times over. The first stage is the arming of the device, when the bias on the pixel is increased above the breakdown voltage. A set delay (the second stage) is then observed, which constitutes the exposure gate. After the gate, a recording pulse is asserted (the third stage) that transfers the state of the pixel (1 or 0) to the readout circuit. Immediately after the recording pulse ends, the pixel is forcefully disarmed (the fourth stage), meaning that the voltage is set below the breakdown voltage. A final delay (the fifth period) is observed after the disarm signal, called the hold-off time. This delay is usually to mitigate afterpulsing events. At the end of the hold-off time the pixel is armed again and the cycle repeats.

In an ideal device, the forced disarm would be unnecessary because avalanches between gates would not affect the occurrence of avalanches during the gates. In practical use, forced disarm is required because of the afterpulsing mechanism, which can induce an avalanche in a subsequent gate with a characteristic exponential decay probability. Figure 2 shows an example of the clocking signals described above.

The dead time associated with these devices is the time between the detected avalanche and the end of the gate, in addition to the hold-off time. To account for this dead time as well as dark current and photon detection efficiency (PDE), (1) is used to calculate the number of photons incident on the detector [8].

$$S = \frac{-\ln\left[\frac{1 - P_{av}}{1 - p_{aft}P_{av}}\right] - \lambda_d}{PDE \cdot t_{gate}} \quad (1)$$

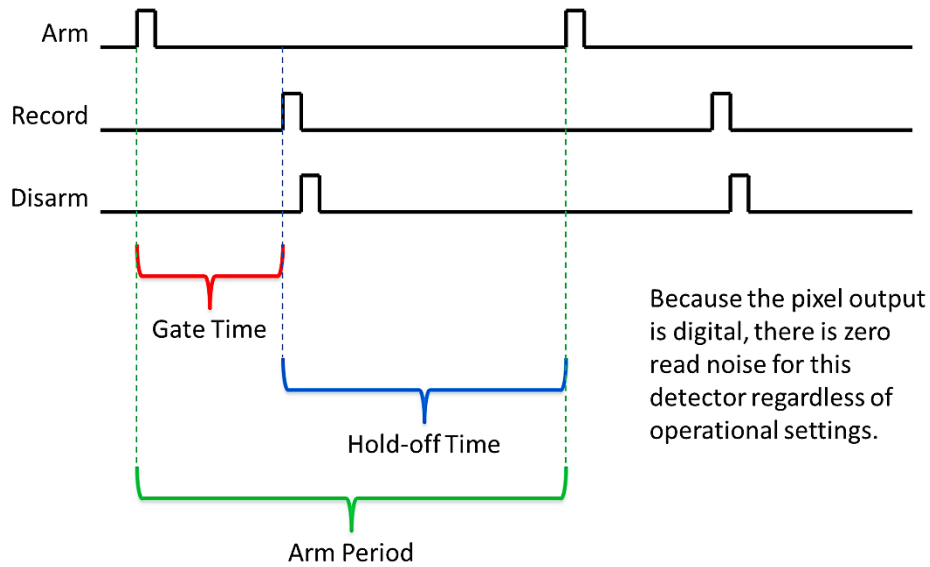


**Figure 2 – This plot shows a sample of the clocking signals required for the GM-APD array operation.**

$S$  is the number of photons incident on each pixel per second,  $P_{av}$  is the avalanche probability (the number of total counts divided by the number of total gates),  $p_{aft}$  is the probability of an afterpulse in a gate, given that the previous gate counted an avalanche, and  $\lambda_d$  is the number of dark current carriers per gate.

#### First-Generation Performance

Testing results for the first-generation devices have been previously reported [6, 9, 10]. The devices were tested prior to, during, and after radiation exposure under a vacuum of  $<1 \mu\text{Torr}$  and at a temperature of 220 K. The detectors were exposed to radiation in a controlled environment at the Massachusetts General Hospital Francis H. Burr Proton Therapy Center. They were irradiated with 60 MeV monoenergetic protons in geometrically-spaced doses for a cumulative dose of 50 krad(Si), the equivalent of 10 solar cycles at an L2 orbit. The detectors were irradiated through a thin aluminum window, which was accounted for in the dose calibration and had a negligible effect on the energy and spatial distributions of the radiation. A summary of the pre- and post-radiation results is provided in Table 1.

#### Radiation Tolerance

EMCCDs experience increases in dark current after radiation damage from two main sources: bulk damage and ionization effects [11]. The latter source is caused by damage at the surface of the devices at the silicon/insulator interface. In GM-APDs, ionization effects do not affect the dark count rate because the avalanche initiation probability for carriers generated at the surface of the device is effectively zero.

**Table 1. SNR modeling characteristics for a GM-APD device at various radiation levels are shown.**

Parameter	Pre-Radiation Value	1 solar cycle	10 solar cycles*
Dark Count Rate (Hz)	38.2	50.7	17.4
PDE (%)	0.3	0.3	0.2
Duty Cycle (%)	97	97	86
Optimum Operating Temperature (K)	160	160	140

\*These data points are for a reduced operating voltage, since afterpulsing dominated the dark signal even at very long (10 ms) hold-off times when the devices were operated at the original voltage setting.

The bulk damage is mostly comprised of deep-level defects (lattice displacement), which act as generation / recombination centers in the material and are very sensitive to changes in temperature [11]. This type of damage is common to both EMCCDs and GM-APDs.

At 160 K, the increase in dark count rate for the GM-APD after one solar cycle (11 years) was  $12.5 \text{ e}^-/\text{s}/\text{pix}$ . In contrast, an x-ray detection CCD device on board the ASCA satellite (with similar shielding and operating temperature) experienced an increase of  $8.8 \text{ e}^-/\text{s}/\text{pix}$  after one solar cycle (assuming that the measurement window was representative of the flux distribution for the entire solar cycle) [12].

#### Improvements and State-of-the-Art Performance

Although the first-generation GM-APD devices had significant dark noise and very low efficiency, a few

simple, targeted improvements would greatly improve their performance. Re-designing the internal device structure would lead to the most significant gains in performance.

As designed, the scupper region in Figure 1 mitigates dark count rate at the expense of efficiency. Even carriers generated by photons in the absorption region have a significant probability of moving to the scupper region. However, the scupper would no longer be necessary if the dark current were not so high.

The high dark current in these devices is due to a number of factors, including damage introduced by thinning the detector. An un-thinned detector with the same internal structure and readout circuitry had a median dark count rate of only 0.03 e<sup>-</sup>/s/pix at 135 K. Current state-of-the-art silicon detectors have dark current on the order of 8 e<sup>-</sup>/s at room temperature (extrapolated to 0.03 e<sup>-</sup>/s at 140 K) [13], achieved through various processing and design improvements. Improving the dark current would eliminate the need for the scupper region and allow a higher fill factor in the device. This would increase the efficiency to the levels seen in other GM-APD devices, near 80%. [14]. Increasing the quality of the substrate will also lead to a decrease in afterpulsing. Ideally, there should be no traps, and therefore no afterpulsing, in a majority of the pixels.

When redesigning the internal structure, care should be taken to keep the volume of the multiplication region as small as possible. Increased volume leads to more carriers participating in each avalanche. This increases optical crosstalk between pixels, which has been measured in GM-APD devices that have large multiplication regions [6]. Significant optical crosstalk leads to large groups of pixels firing during a single gate, which makes signal estimation nearly impossible. In order to mitigate the effects of a larger multiplication area, which must occur if the active area is expanded, optical and electrical isolation features should be added between pixels.

#### 4. EXOPLANET DETECTION SIMULATIONS

One way to evaluate the performance of the EMCCD and GM-APD for exoplanet imaging is to compare the signal-to-noise ratio (SNR) of each device across a range of relevant signal levels. The theoretical SNR equations for the EMCCD in photon-counting mode and the GM-APD are actually the same in certain circumstances. The EMCCD must be operated with a detection threshold at least three times that of the read noise (in order to avoid significant counts from read noise) and at least 10 times smaller than the total gain (to avoid lost signal due to high thresholding).

The GM-APD must be operated with a hold-off time such that the afterpulsing probability is zero. If all of these assumptions are true, then (2) gives the theoretical SNR of both an EMCCD in photon-counting mode and a GM-APD [8].

$$SNR = \frac{\eta \cdot \lambda_p \cdot n_{gates}}{\sqrt{\frac{p}{(1-p)} \cdot n_{gates}}} \quad (2)$$

$$\text{where } p = 1 - e^{-(\eta \cdot \lambda_p + \lambda_d)}$$

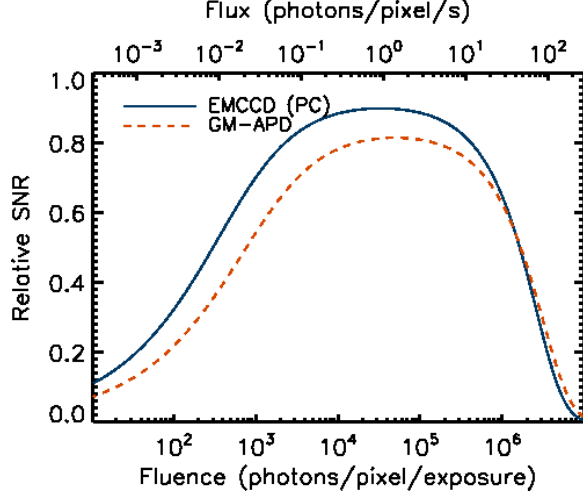
$\eta$  is the efficiency of the detector (QE for EMCCDs and PDE for GM-APDs),  $\lambda_p$  is the number of incident photons per gate,  $\lambda_d$  is the number of dark current carriers per gate (for an EMCCD, this includes CIC),  $n_{gates}$  is the number of gates in the exposure, and  $p$  is the avalanche probability.

Table 2 gives the relevant performance parameters for both detectors. The values for the EMCCD are taken from the manufacturer [5] and from projected use in the WFIRST-AFTA mission [4]. The GM-APD parameter values are based on the state-of-the-art performance metrics detailed in Section 3 and the same use as the EMCCD.

**Table 2. Performance parameters for two devices are shown: an e2v CCD201-20 EMCCD in photon-counting mode and a GM-APD array.**

Parameter (units)	EMCCD (PC)	GM-APD
QE / PDE (%)	93	70
Dark Current (e <sup>-</sup> /pix/s)	0.0003	0.03
CIC (e <sup>-</sup> /pix/frame)	0.001	0
Duty Cycle (%)	100	99.98
Gate Time (ms)	55	55
Read Noise (e <sup>-</sup> rms/frame)	0.04 (effective)	0

Figure 3 shows the SNR of the EMCCD and the GM-APD over a range of signal levels. The simulated exposure time is 10 hours in the V-band (550 nm), and the signal level is per pixel, not per object. Each exposure is made up of 55 ms, and the GM-APD has a hold-off time of 10  $\mu$ s.



**Figure 3** – This plot shows the simulated results for an e2v CCD201-20 operated in photon-counting mode and a GM-APD array. Relative SNR is the SNR normalized to the shot noise limit. Both detectors have the same gate time and exposure settings, but unique efficiency and noise values. The total exposure time is 10 hours.

The EMCCD has a wider range of high SNR than the GM-APD does due to its lower dark noise, and it also has a higher peak due to its higher efficiency. To illustrate the implications of the difference in SNR, Figure 4 shows the wall time required to reach an SNR of 10 for both detectors given the settings described above.

While the results in Figure 3 and Figure 4 are useful for comparison, they do not consider the imaging or spectroscopy cases, where the light from the object is spread across multiple pixels. In an imaging scenario, assuming that the focal spot size is diffraction-limited, (3) gives the angular width (in radians) of the central lobe of the airy disk pattern (between the first dark minima).

$$\theta = 2.44 \frac{\lambda}{D} \quad (3)$$

$\lambda$  is the wavelength of the light and  $D$  is the diameter of the aperture. The WFIRST-AFTA coronagraph aperture is 2.4 m and the plate scale is 17 mas/pix [4], so the central lobe of the diffraction pattern at 550 nm is 115 mas or 6.78 pixels. Alternatively, the full width at half maximum (FWHM) can be calculated using (4).

$$\theta = 1.03 \frac{\lambda}{D} \quad (4)$$

The FWHM is 48.7 mas, or 2.86 pixels, at 550 nm. Figure 5 shows a 1D cross-section of the diffraction-limited, airy disk point spread function (PSF). The

solid line shows the theoretical function and the dashed line shows the function as sampled by the pixels in the simulated sub-array.

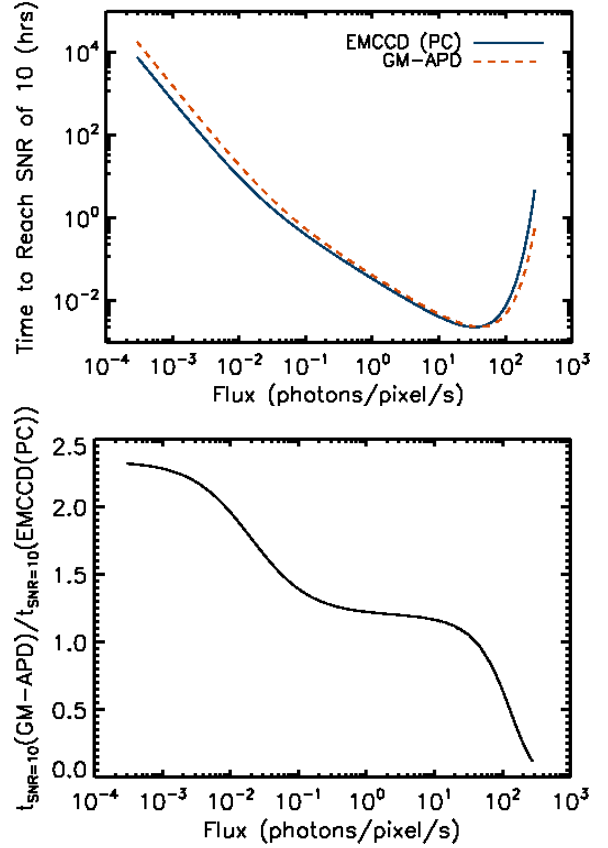


**Figure 4** – This plot shows the wall time required to reach SNR= 10 (top) and the ratio of time required for the two detectors (bottom).

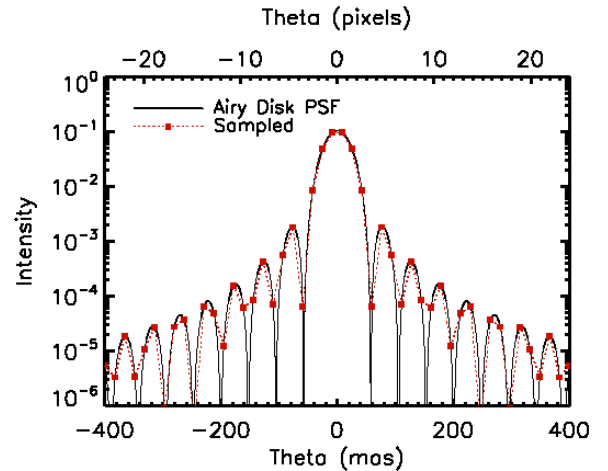


**Figure 5** – This plot shows a 1D cut of the simulated PSF for the WFIRST coronagraph instrument. The solid line is the theoretical PSF and the dashed line is the PSF as sampled by the detectors (17 mas/pix).

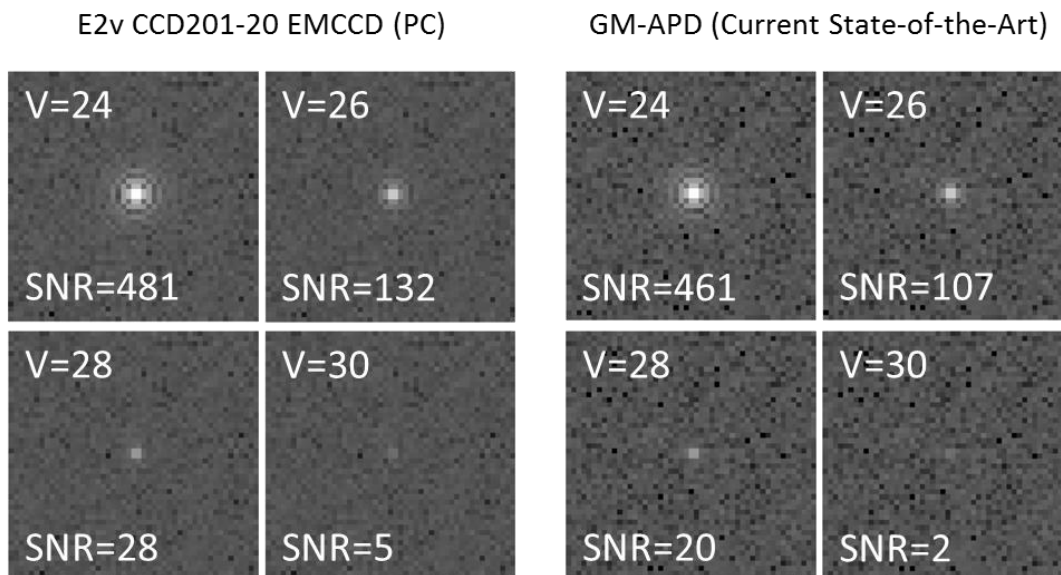


**Figure 6 – This plot shows simulated images of exoplanets of varying magnitudes for an EMCCD (left) in photon-counting mode and a GM-APD (right). The corresponding apparent magnitude in the V band for each simulation is noted in the top left corner of each image.**

Figure 6 shows simulated images of exoplanets with various magnitudes for both the EMCCD and the GM-APD. The simulated images assume that the planet is not in a debris field and that any remaining diffracted light from the star is not significant. Zodiacal light is assumed to be negligible as well.

The background noise is notably greater for the GM-APD, which has a total dark noise contribution of  $0.0017 \text{ e}^-/\text{pix}/\text{gate}$  compared to the EMCCD's combined dark current and CIC of  $0.0011 \text{ e}^-/\text{pix}/\text{gate}$ . While both detectors resolve the first few maxima of the signal for the brightest planet ( $V = 24$ ), the EMCCD does notably better for the faintest planet ( $V = 30$ ) due to a combination of lower dark noise and higher efficiency.

## 5. CONCLUSIONS

The first-generation GM-APD array-based detectors demonstrated zero read noise and modest afterpulsing at temperatures above 140 K. Radiation-induced dark current was 1.4x higher than that of a CCD with the same radiation dose and shielding. However, the devices had high dark current and low efficiency. The dark current contribution was  $38 \text{ e}^-/\text{s}/\text{pix}$ , and the PDE was only 0.3% at its peak. However, the causes of these shortcomings are known, and a second generation of devices is currently being tested that have addressed the problems [6].

The state-of-the-art GM-APD performance is roughly equivalent to the EMCCD for fluxes greater than 1 photon/s (see Figure 4) when considering the time required to reach an SNR of 10. While GM-APD performance lags behind EMCCDs for lower signal levels, targeted research to reduce the dark current would significantly improve SNR for faint objects. Given the limitation of CIC in EMCCDs, GM-APDs with dark current comparable to state-of-the-art CCD levels would offer an advantage for low-light-level imaging and spectroscopy. Figure 7 shows the theoretical SNR of a GM-APD with various dark current values. The lowest simulated value is equal to that of an EMCCD ( $0.0003 \text{ e}^-/\text{s}/\text{pix}$ ). Because the EMCCD has CIC noise due to high pixel readout rates, the GM-APD performance at the lower light levels exceeds that of the EMCCD even with only a modest decrease in the dark current to  $0.01 \text{ e}^-/\text{s}/\text{pix}$ .

The improvement in SNR shown in Figure 7 is also evident when comparing the time required to reach an SNR of 10 for the GM-APD device and the e2v EMCCD (see Figure 8).

A shot-noise-limited detector would reach an SNR of 10 in 10 hours for a fluence of 100 photons ( $0.003 \text{ photons/s}$ ). The e2v EMCCD in photon-counting mode would require 94.7 hours and a GM-APD with the same dark current would require only 16.3 hours. With current state-of-the-art dark current, the GM-APD would require 207.8 hours (2.2x the exposure time required for the EMCCD), though a

GM-APD with a 3x decrease in dark current to  $0.01 \text{ e}^-/\text{s}/\text{pix}$  would require 85.8 hours – less than the EMCCD.

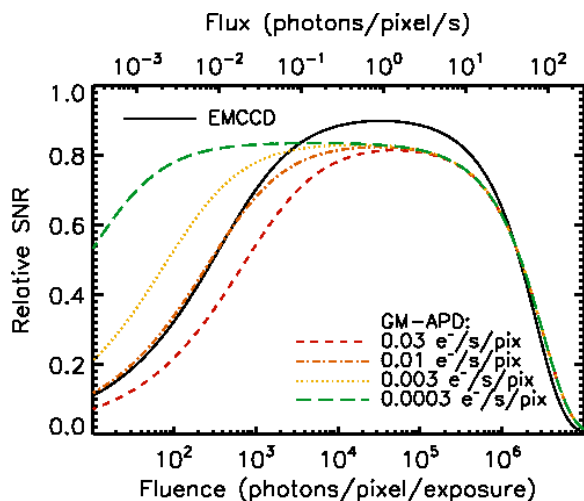


**Figure 7 – This plot shows the relative SNR of an e2v EMCCD in photon-counting mode and a theoretical GM-APD device with dark current equal to that of the EMCCD. Both detectors have the same gate time and exposure time settings.**

The total exposure time is 10 hours. The  $0.03 \text{ e}^-/\text{s}/\text{pixel}$  curve is the current state-of-the-art.

A shot-noise-limited detector would reach an SNR of 10 in 10 hours for a fluence of 100 photons ( $0.003 \text{ photons/s}$ ). The e2v EMCCD in photon-counting mode would require 94.7 hours and a GM-APD with the same dark current would require only 16.3 hours. With current state-of-the-art dark current, the GM-APD would require 207.8 hours (2.2x the exposure time required for the EMCCD), though a GM-APD with a 3x decrease in dark current to  $0.01 \text{ e}^-/\text{s}/\text{pix}$  would require 85.8 hours – less than the EMCCD.

Improvements in PDE could bring GM-APD efficiency closer to that of EMCCDs, though avalanche initiation probability limits the total efficiency.

The GM-APD devices also have similar radiation tolerance to existing CCD devices. While the ASCA satellite CCD experienced less radiation damage when compared to an equivalent simulated environment for the GM-APD, the latter are not susceptible to surface-generated dark current. This gives them the potential to surpass the CCD's radiation tolerance with targeted design improvements. Increased shielding, such as on the STIS instrument on HST, can also significantly decrease the radiation dose per year and the

radiation-induced dark current [15]. Another effect of radiation damage on CCD-based devices (including EMCCDs) is a decrease in the charge transfer efficiency (CTE) [16, 17]. GM-APDs are not affected by CTE, and so are immune to CTE-related decreases in performance.

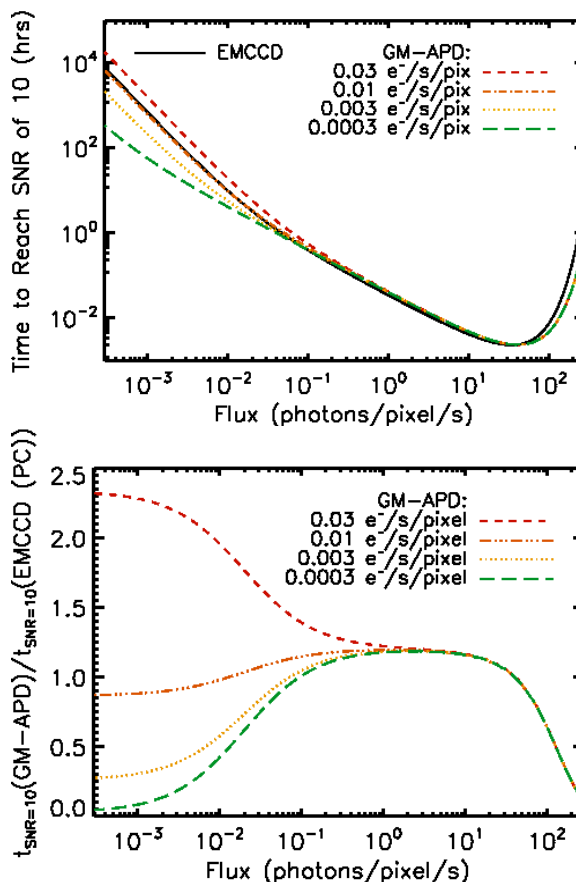


**Figure 8 – This plot shows the wall time required to reach SNR= 10 (top) and the ratio of time required (bottom) for the e2v EMCCD and the theoretical GM-APD with dark current equal to that of the EMCCD. The  $0.03 \text{ e}^-/\text{s}/\text{pixel}$  curve is the current state-of-the-art.**

State-of-the-art performances for GM-APDs lag significantly behind that of EMCCDs for low fluxes ( $< 1 \text{ photon/s}$ ), but are roughly equivalent at higher fluxes, as shown in Figure 3 and Figure 4. The only difference in performance at fluxes greater than 1 photon/s is the lower efficiency associated with GM-APDs due to non-ideal avalanche initiation probability. However, improvements in dark current could increase the performance of the GM-APD at low signal levels. If the dark current were improved by an order of magnitude, the performance of the GM-APD is higher for fluxes less than 0.1 photons/s, as shown in Figure 7 and Figure 8. EMCCDs are

fundamentally limited by CIC noise, which only increases as the number of pixels increases for large-format arrays due to high pixel readout rates. Theoretically, GM-APD devices are less limited by fundamental noise sources for extremely low signal levels and may ultimately be the better solution with more advanced research.

## REFERENCES

- [1] N. C. Santos, "Extra-solar planets: Detection methods and results," *New Astronomy Reviews*, vol. 52, no. 2, pp. 154-166, 2008.
- [2] C. A. Grady, C. R. Proffitt, E. Malumuth, B. E. Woodgate, T. R. Gull, C. W. Bowers, S. R. Heap, R. A. Kimble, D. Lindler, P. Plait and A. Weinberger, "Coronagraphic Imaging with the Hubble Space Telescope and the Space Telescope Imaging Spectrograph," *Publications of the Astronomical Society of the Pacific*, vol. 115, no. 811, pp. 1036-1049, 2003.
- [3] V. G. Ford, D. Lisman, S. B. Shaklan, T. Y. Ho, A. Kissil, E.-Y. Kwack and A. Lowman, "The Terrestrial Planet Finder coronagraph: technology and mission design studies," *Astronomical Telescopes and Instrumentation*, pp. 1274-1283, 2004.
- [4] NASA, "WFIRST-AFTA Science Definition Team Interim Report," 30 April 2014. [Online]. Available: [http://wfirst.gsfc.nasa.gov/science/sdt\\_public/WFIRST-AFTA\\_SDT\\_Interim\\_Report\\_April\\_2014.pdf](http://wfirst.gsfc.nasa.gov/science/sdt_public/WFIRST-AFTA_SDT_Interim_Report_April_2014.pdf). [Accessed 9 October 2014].
- [5] e2v technologies, "CCD201-20 Back Illuminated 2-Phase IMO Series Electron Multiplying CCD Sensor," e2v technologies (uk) limited, Chelmsford, Essex, UK, Nov. 2011.
- [6] D. Figer and K. Kolb, "A Photon-Counting Detector for Exoplanet Missions," *Technology Development for Exoplanet Missions: Technology Milestone Report*, JPL Document, no. D-93392, 2014.
- [7] B. F. Aull, D. R. Schuette, R. K. Reich and R. L. Johnson, "Adaptive optics wavefront sensors based on photon-counting detector arrays," in *Proc. of SPIE, Adaptive Optics Systems II*, San Diego, USA, 2010.
- [8] K. Kolb, "Signal-to-noise ratio of Geiger-mode avalanche photodiode single-photon counting imaging detectors," *Optical Engineering*, vol. 53, no. 8, p. 081904, 2014.
- [9] K. Kolb, B. Hanold, J. Lee and D. F. Figer, "Evaluation of GM-APD array devices for low-light-level imaging," in *SPIE Sensing Technology + Applications*, Baltimore, MD, 2014.
- [10] K. Kolb, B. Hanold, J. Lee and D. F. Figer, "Test Results for an Array-Based GM-APD Detector Before and After Irradiation," in *Proceedings of the Scientific Detector Workshop*, Florence, 2013.
- [11] J. Janesick, T. Elliott and F. Pool, "Radiation Damage in Scientific Charge-Coupled Devices," *IEEE Transactions on Nuclear Science*, vol. 36, no. 1, pp. 572-578, 1989.
- [12] A. Yamashita, T. Dotani, M. Bautz, G. Crew, H. Ezuka, K. Gendreau, T. Kotani, K. Mitsuda, C. Otani, A. Rasmussen, G. Ricker and H. Tsunemi, "Radiation Damage to Charge Coupled Devices in the Space Environment," *IEEE Transactions on Nuclear Science*, vol. 44, no. 3, pp. 847-853, June 1997.
- [13] J. C. Jackson, A. P. Morrison, D. Phelan and A. Mathewson, "A Novel Silicon Geiger-Mode Avalanche Photodiode," in *IEDM*, San Francisco, USA, 2002.
- [14] D. Renker and E. Lorenz, "Advances in solid state photon detectors," *Journal of Instrumentation*, vol. 4, no. 4, p. P04004, April 2009.
- [15] R. A. Kimble, P. Goudfrooij and R. L. Gilliland, "Radiation damage effects on the CCD detector of the Space Telescope Imaging Spectrograph," in *Proc. of SPIE: UV, Optical, and IR Space Telescopes and Instruments*, Munich, Germany, 2000.
- [16] K. Mori, U. Nishioka, S. Ohura, Y. Koura, M. Yumauchi, H. Nakajima, S. Ueda, H. Kan, N. Anabuki, R. Nagino, K. Hayashida, H. Tsunemi, T. Kohmura, S. Ikeda, H. Murakami, M. Ozaki, T. Dotani, Y. Maeda and K. Sagara, "Proton radiation damage experiment on P-Channel CCD for an X-ray CCD camera onboard the ASTRO-H satellite," *Nuclear Instruments and Methods in Physics Research A*, vol. 731, pp. 160-165, 2013.
- [17] J. Janesick, G. Soli, T. Elliott and S. Collins, "The Effects of Proton Damage on Charge-Coupled Devices," in *Proc. of SPIE: Charge-Coupled Devices and Solid State Optical Sensors II*, San Jose, USA, 1991.

## BIOGRAPHY



**Kimberly Kolb** is a Ph.D. student at the Rochester Institute of Technology. She received her B.E. degree in Microelectronic Engineering in 2008 from the Kate Gleason College of Engineering at the Rochester Institute of Technology (RIT), and her M.S. in Imaging Science from the Chester F.

Carlson Center for Imaging Science at the same university in 2011. Kolb won a NASA Earth and Space Science Fellowship for her dissertation proposal, "Single Photon-Counting Detectors for NASA Astronomy Missions," wherein she proposes to evaluate and compare three types of semiconductor-based photon-counting detectors: Geiger-mode APDs, linear-mode APDs, and EMCCDs. Kolb plans to complete her PhD in Imaging Science at the Center for Detectors in the spring of 2015.



**Don Figer** is the Director of the Center for Detectors (CfD) and a Professor at RIT. He received a B.S. in Physics/Math/Astronomy from Northwestern University in 1989, a M.S. in Astronomy from the University of Chicago in 1992, and a Ph.D. in Astronomy from UCLA in 1995. He became a Professor at RIT

in 2006 and served as the director of the Rochester Imaging Detector Laboratory (RIDL). Figer founded the CfD in 2010, consisting of RIDL, the Imaging LIDAR Laboratory, the Quantum Dot Detector Laboratory, and the Wafer Probe Station Laboratory. He has been the P.I. of several successful grant proposals, most recently with NSF ATI and NASA APRA funding for HgCdTe IR detectors grown on silicon substrates. The projects will evaluate and improve the detector technology to achieve high performance at low cost. Prior to his current appointments at RIT, he worked at Space Telescope Science Institute as an Associate Astronomer.